Int. J. Heat Mass Transfer. Vol. 24, No. 10, pp. 1611–1620, 1981
Printed in Great Britain

0017-9310/81/101611-10 $02.00/0

HEAT TRANSFER THROUGH SINGLE AND DOUBLE VERTICAL WALLS IN NATURAL CONVECTION: THEORY AND EXPERIMENT

REN ANDERSON and ADRIAN BEJAN
Department of Mechanical Engineering,
University of Colorado, Boulder, CO 80309, U.S.A.

(*Received* 8 *December* 1980 *and in revised form* 18 *February* 1981)

Abstract – The heat transfer through vertical partitions surrounded by thermally-stratified fluids is studied theoretically and experimentally. The theory is based on the Oseen linearization method. The analytical results show the effect of thermal stratification on the partition temperature, fluid flow and heat flux. The relationship between overall heat transfer (Nusselt number) and the degrees of thermal stratification on both sides of the partition is determined. The experimental part of the study confirms the heat transfer features predicted analytically. In particular, it is shown that the theoretical Nusselt number calculation is in good agreement with experimental measurements. It is shown also that the net heat transfer between the two ends of a rectangular enclosure is proportional to $(1+n)^{-0.61}$, where n is the number of vertical partitions inserted in the middle of the enclosure.

NOMENCLATURE

- A, vertical temperature gradient in the hot reservoir, $a=AH/\Delta T$;
- B, vertical temperature gradient in the cold reservoir, $b=BH/\Delta\hat{T}$;
- g, gravitational acceleration;
- H, partition height;
- k, thermal conductivity;
- l, horizontal length scale;
- Nu, Nusselt number, hH/k_f;
- p, even function of x;
- Pr, Prandtl number;
- q, odd function of x;
- Ra, Rayleigh number, $g\beta H^3\Delta T/(\nu\alpha)$;
- t_0, partition temperature;
- T, temperature;
- U, vertical velocity;
- V, horizontal velocity;
- W, wall thickness;
- X, vertical position;
- Y, horizontal position.

Greek letters

- α, thermal diffusivity;
- β, coefficient of thermal expansion;
- ν, kinematic viscosity;
- ϕ, local fluid temperature gradient.

Subscripts

- C, ambient conditions on the cold (right-hand) side of the partition;
- f, fluid;
- H, ambient conditions on the hot (left-hand) side of the partition;
- w, wall.

Superscripts

- $\hat{}$, based on the temperature difference between reservoirs, evaluated at mid-height;
- $*$, based on the temperature difference between the end plates.

1. INTRODUCTION

THE TASK of conserving energy in buildings requires a solid understanding of the fluid mechanics and heat transfer phenomena responsible for the leakage of heat through building walls. To a large extent, these phenomena are driven by the buoyancy effect of temperature differences existing between various parts of the building. One of the least understood, yet most frequent situations, involves the transfer of heat through vertical walls which separate adjacent rooms at different temperatures. This basic configuration is the focus of our study.

Analytically, the problem of heat transfer through a vertical wall is a difficult one, in the sense that the wall temperature condition is one of the unknowns of the problem. The wall temperature is one of the results of the interaction between the natural boundary layers which form on both sides of the wall. It is due to this analytical difficulty that the previous analytical studies of the natural convection near vertical surfaces relied on simplifying assumptions concerning conditions of the wall. These simplifications have included constant wall temperature [1], constant heat flux through the wall [2], and a power-law wall temperature distribution [3]. The same approximations have been made for heat transfer through rectangular enclosures. The classical enclosure model consists of two isothermal vertical walls facing each other [4]. Lock and Ko [5] and Anderson and Bejan [6] have produced more realistic results by studying the transfer of heat across a vertical wall separating two fluid reservoirs at uniform temperatures, without making assumptions about temperature distributions or heat flux at the wall surface.

The objective of this paper is to report a fundamental study of the transfer of heat through a single or a double partition which divides a rectangular enclosure into two differentially-heated chambers. This is the most basic configuration which simulates the thermal interaction between adjacent rooms in an actual building.

This study has two parts. The first part presents a theory which predicts the temperature and velocity field around a single partition sandwiched between fluid reservoirs with thermal stratification in the vertical direction. The thermal stratification is a common feature of adjacent, finite-size, enclosures filled with fluid and separated by a heat conducting partition. This feature is confirmed by the experimental phase of our study presented in the second half of this paper. In addition to illustrating the temperature distribution and fluid circulation through the two-chamber system, the experimental part reports much-needed information regarding the overall heat transfer through single or double partitions which divide rectangular spaces filled with fluid.

The experimental apparatus was specifically designed to simulate high Rayleigh number flows, as in actual buildings ($Ra \sim 10^9$, 10^{10}). Using water as the working fluid, we were able to achieve the desired Rayleigh number range in a desk-size experimental chamber. The Prandtl number discrepancy between water ($Pr = 6$) and air ($Pr = 0.7$) is known to have only a small effect on overall heat transfer calculations. This effect was illustrated by Raithby, Hollands and Unny [7] for vertical enclosures, and by Anderson and Bejan [6] for overall heat transfer through a vertical wall separating fluids at different temperatures.

2. THEORY

2.1. *Mathematical formulation*

Consider a vertical impermeable wall of height H and thickness W, as shown in Fig. 1. This partition separates two thermally-stratified reservoirs

$$T_H = \hat{T}_H + AX \tag{1}$$

$$T_C = \hat{T}_C + BX \tag{2}$$

where A and B are the respective temperature gradients in the vertical direction. Temperatures $\hat{T}_H$ and $\hat{T}_C$ are the two reservoir temperatures evaluated at mid-height ($X = 0$). We focus on the boundary layer regime where, as shown in Fig. 1, the sides of the vertical partition are lined by two buoyancy-driven layers in counterflow.

The equations governing the steady-state conservation of mass, momentum and energy can be written as

$$\frac{\partial u}{\partial x} + \frac{\partial v}{\partial y} = 0 \tag{3}$$

$$\frac{\partial^3 u}{\partial y^3} = -\frac{\partial t}{\partial y} \tag{4}$$

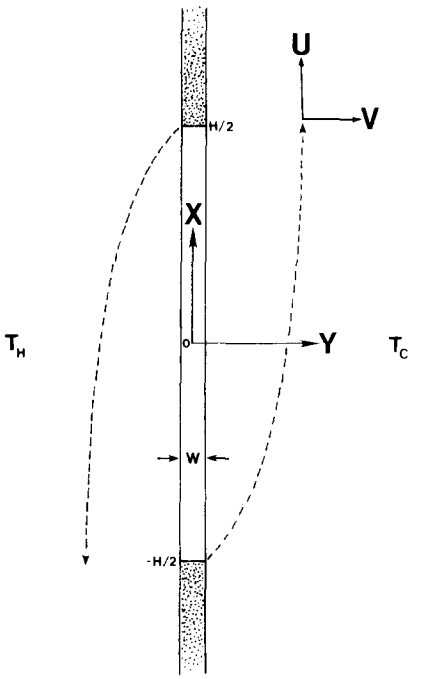

FIG. 1. Schematic of a single partition surrounded by fluids at different temperatures.

$$u\frac{\partial t}{\partial x} + v\frac{\partial t}{\partial y} = \frac{\partial^2 t}{\partial y^2} \tag{5}$$

with the corresponding boundary conditions

$$u = v = 0 \quad \text{and} \quad t = t_0(x) \quad \text{at } y = 0 \tag{6}$$

$$t = \tfrac{1}{2} + ax \quad \text{and} \quad u = 0 \quad \text{as } y \to -\infty$$

$$t = -\tfrac{1}{2} + bx \quad \text{and} \quad u = 0 \quad \text{as } y \to +\infty. \tag{7}$$

Equations (3)–(5) are based on the Boussinesq and boundary layer approximations; they appear in dimensionless form, based on the following definitions

$$x = X/H, \quad y = Y/l \tag{8}$$

$$u = \frac{Ul^2}{\alpha H}, \quad v = \frac{Vl}{\alpha} \tag{9}$$

$$t = [T - (\hat{T}_H + \hat{T}_C)/2]/(\hat{T}_H - \hat{T}_C) \tag{10}$$

$$l = H\hat{Ra}^{-1/4} \tag{11}$$

$$\hat{Ra} = \frac{g\beta H^3(\hat{T}_H - \hat{T}_C)}{\alpha\nu}. \tag{12}$$

As shown in detail by Gill [8], scaling (8)–(12) is based on the balance between the convective and conductive terms in the energy equation, and on the balance between the buoyancy and diffusion terms in the momentum equation. It was further assumed that the boundary layer is thin, i.e. $H \gg l$ or $Ra \gg 1$. In addition, the inertia terms have been ignored in equation (4) by assuming $Pr > 1$. The large Pr approximation is valid for liquids such as water and oil, invalid for liquid metals, and approximately valid for gases. Anderson and Bejan [6] have estimated the error associated with applying the $Pr > 1$ theory to air:

they found that this theory overestimates the Nusselt number by approximately 10%.

The partition temperature distribution $t_0(x)$, equation (6), is one of the unknowns in this heat-transfer problem. The temperature drop across the solid partition is considered negligible in comparison with the temperature difference between the two semi-infinite fluid reservoirs: this assumption is valid in the limit

$$\frac{k_w H}{k_f W \widehat{Ra}^{1/4}} \gg 1 \tag{13}$$

i.e. in the limit where the thermal conductance through the solid wall (k_w/W) is much greater than the conductance through one of the boundary layers (k_f/l).

2.2. *Linearized analytical solution*

We have shown previously [6] that the nonlinearity associated with the convective terms in the energy equation (5) can be removed by replacing $\partial t/\partial x$ and v with unknown functions of altitude, x. The unknown functions are to be determined later from integral conditions. This technique was first applied to problems involving natural convections in enclosures by Ostrach [4] and by Gill [8]. As shown in a recent compilation of results for heat transfer across vertical enclosures, Gill's linearized theory predicts very well the overall heat-transfer rate [9].

Following an analytical course identical to the one outlined in [6], the linearized analytical solution to equations (3)–(5), subject to conditions (6) and (7) can be expressed as

$$u_C = \frac{-(t_0 + \frac{1}{2} - bx)}{\lambda_1^2 - \lambda_2^2}\left[e^{\lambda_1 y} - e^{\lambda_2 y}\right] \tag{14}$$

$$u_H = \frac{-(t_0 - \frac{1}{2} - ax)}{\xi_1^2 - \xi_2^2}\left[e^{-\xi_1 y} - e^{-\xi_2 y}\right] \tag{15}$$

$$t_C = \frac{(t_0 + \frac{1}{2} - bx)}{\lambda_1^2 - \lambda_2^2}\left[\lambda_1^2 e^{\lambda_1 y} - \lambda_2^2 e^{\lambda_2 y}\right] - \tfrac{1}{2} + bx \tag{16}$$

$$t_H = \frac{(t_0 - \frac{1}{2} - ax)}{(\xi_1^2 - \xi_2^2)}\left[\xi_1^2 e^{-\xi_1 y} - \xi_2^2 e^{-\xi_2 y}\right] + \tfrac{1}{2} + ax. \tag{17}$$

Subscripts C and H denote the cold side and hot side of the solid partition. Defining

$$p = \lambda_1 + \lambda_2 + \xi_1 + \xi_2 \tag{18}$$

$$q = v/p \tag{19}$$

it can be shown that

$$\lambda_{1,2} = \tfrac{1}{4}p(1 + q)[1 \pm i\sqrt{(1 - 2q)}] \tag{20}$$

$$\xi_{1,2} = \tfrac{1}{4}p(1 - q)[1 \pm i\sqrt{(1 + 2q)}]. \tag{21}$$

The analytical solution (14)–(21) can be recast into a physically more meaningful form by introducing the new variables

$$K = \tfrac{1}{4}p(1 + q), \quad L = K\sqrt{(1 - 2q)} \tag{22}$$

$$M = \tfrac{1}{4}p(1 - q), \quad N = M\sqrt{(1 + 2q)}. \tag{23}$$

In terms of these new variables, the vertical velocity and temperature profiles across the boundary layers assume the form

$$u_C = \frac{-(t_0 + \frac{1}{2} - bx)e^{Ky}}{2KL}\sin(Ly) \tag{24}$$

$$u_H = \frac{-(t_0 - \frac{1}{2} - ax)e^{-My}}{2MN}\sin(-Ny) \tag{25}$$

$$t_C = \frac{(t_0 + \frac{1}{2} - bx)}{2KL} \times e^{Ky}[2KL\cos(Ly) + (K^2 - L^2)\sin(Ly)] - \tfrac{1}{2} + bx \tag{26}$$

$$t_H = \frac{(t_0 - \frac{1}{2} - ax)e^{-My}}{2MN} \times [2MN\cos(-Ny) + (M^2 - N^2)\sin(-Ny)] + \tfrac{1}{2} + ax. \tag{27}$$

These expressions show that the velocity and temperature profiles are oscillatory in nature, with exponentially decaying amplitudes.

Substituting expressions (26) and (27) into the heat flux continuity statement

$$\frac{\partial t_C}{\partial y} = \frac{\partial t_H}{\partial y} \quad \text{at} \quad y = 0 \tag{28}$$

yields an equation for the unknown partition temperature $t_0(x)$ in terms of a, b, and $q(x)$

$$t_0 = \frac{ax(1 - q)^2 + bx(1 + q)^2 - 2q}{2(1 + q^2)}. \tag{29}$$

Limits are established on $q(x)$ by recalling that $H \gg l$, hence, in this limit, the two boundary layers function like a very long counterflow heat exchanger. In this counterflow, the inlet temperatures of the two streams are fixed by the reservoir temperatures; therefore

$$t_0 = (a + 1)/2, \quad q = -1 \quad \text{at } x = \tfrac{1}{2} \tag{30}$$

$$t_0 = -(b + 1)/2, \quad q = 1 \quad \text{at } x = -\tfrac{1}{2}. \tag{31}$$

The remaining unknown functions, $q(x)$ and $p(x)$, are determined from integral versions of the energy equation for both boundary layers

$$\frac{d}{dx}\left(\int_0^\infty u_C t_C \, dy\right) + |v_C t_C|_0^\infty = \left|\frac{\partial t_C}{\partial y}\right|_0^\infty \tag{32}$$

$$\frac{d}{dx}\left(\int_{-\infty}^0 u_H t_H \, dy\right) + |v_H t_H|_{-\infty}^0 = \left|\frac{\partial t_H}{\partial y}\right|_{-\infty}^0. \tag{33}$$

The resulting integral conditions are

$$\frac{d}{dx}\left[\frac{(1 - q)^4}{(1 + q^2)^2 p^3 (1 + q)^3}\right] = \frac{(1 - q)^2}{(1 + ax - bx)(1 + q^2)} \times \left[\frac{p(1 + q)^2}{q} - \frac{2b}{p^3(1 + q)^3(1 - q)} - \frac{2(1 - q)^2(a - b)}{(1 + q^2)p^3(1 + q)^3}\right] \tag{34}$$

$$\frac{d}{dx}\left[\frac{(1+q)^4}{(1+q^2)p^3(1-q)^3}\right]=\frac{(1+q)^2}{(bx-1-ax)(1+q^2)}\times\left[\frac{p(1-q)^2}{q}-\frac{2a}{p^3(1-q)^3(1+q)}-\frac{2(1+q)^2(b-a)}{(1+q^2)p^3(1-q)^3}\right]. \quad (35)$$

In conclusion, the analytical solution (24)–(27) depends on three unknown functions of altitude (t_0, q and p) to be determined from equations (29), (34) and (35). Note that equations (34) and (35) have the form $dC/dx=D$ and $dE/dx=F$ which, divided side by side, yield $dC/dE = D/F$. These equations were integrated numerically. Starting at the top or at the bottom of the partition, an initial guess was made for the starting value p_0 corresponding to $x=\mp\frac{1}{2}$ and $q = \pm 1$. After decreasing q by a small amount dq, the equation $dC/dE = D/F$ was used to evaluate the change in p, while equation (34) was used to evaluate the change in x. This process was repeated, trying new guesses for p_0, until conditions (30) and (31) were satisfied at the opposite end of the partition. The stepsize dq was adjusted until the results agreed with those reported in [6] for the limiting case $a = b = 0$.

2.3. *Temperature, velocity and heat-transfer results*

In order to highlight the effect of thermal stratification on the heat-transfer phenomenon, the results of the preceeding analysis are presented for the case of uniform hot reservoir temperature ($a = 0$) and varying degrees of cold reservoir stratification (b). The levels of stratification in the cold fluid are shown in Fig. 2 along with the temperature distribution on the surface of the partition. The partition profile is approximately linear over most of its height, with large gradients at the top and bottom where the boundary layer approximation no longer applies. The profiles on the partition surface are centered around the mean temperature $(\hat{T}_H + \hat{T}_C)/2$ and have smaller slopes than the profiles within the cold fluid. The partition is warmer in the upper half and colder in the bottom half than it would have been without stratification.

Velocity profiles at mid-height are reported in Fig. 3 and corresponding temperatures in Fig. 4. Increasing the stratification decreases the boundary layer velocity on both sides of the partition. As can be seen from Fig. 4, the incoming hot fluid is not cooled as rapidly when the cold reservoir is stratified. This warmer fluid is not as dense and therefore descends more slowly. A related mechanism is responsible for the reduced flow on the cold side of the partition. Even though the incoming cold fluid is heated by the same amount regardless of stratification level, the temperature in the fluid reservoir also increases when the reservoir is stratified. This leads to a net reduction in the local buoyancy force.

The profiles of Figs. 3 and 4 exhibit weak temperature inversions and flow reversals at the outer edge of the boundary layer. Eichorn [10] and Jaluria and Gebhart [11] report that these effects are accentuated as the Prandtl number is increased. Since the present study assumes $Pr > 1$, as for water, the profiles shown in Figs. 3 and 4 are probably not representative of the physics of small Prandtl number fluids.

An examination of the heat flux distribution along the partition explains why the temperature profiles within the cold reservoir are relatively independent of the level of stratification (see Fig. 5). Even though flow velocities are reduced, there is a net increase in the total heat flow, the increase being concentrated at the bottom of the partition. The lower temperature of the incoming fluid is compensated by an increased heating rate so that the temperature profile at midheight remains unchanged.

A summary of the effect of stratification upon the overall heat transfer between reservoirs is shown in Fig. 6, with a summary of representative values in Table 1. The solid lines correspond to the case of constant stratification in the cold fluid. The dashed line indicates the locus of equal levels of hot and cold fluid stratification. As indicated previously in Fig. 5, in-

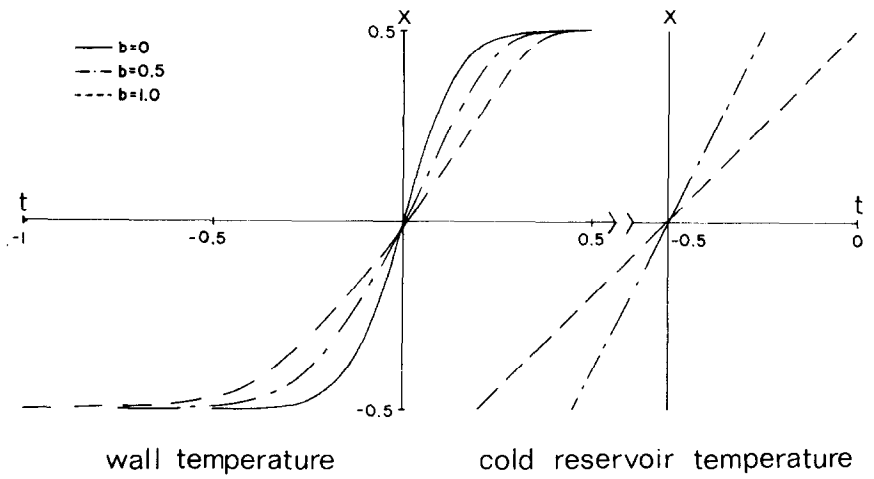

FIG. 2. The effect of reservoir stratification on partition temperature (the hot reservoir is isothermal).

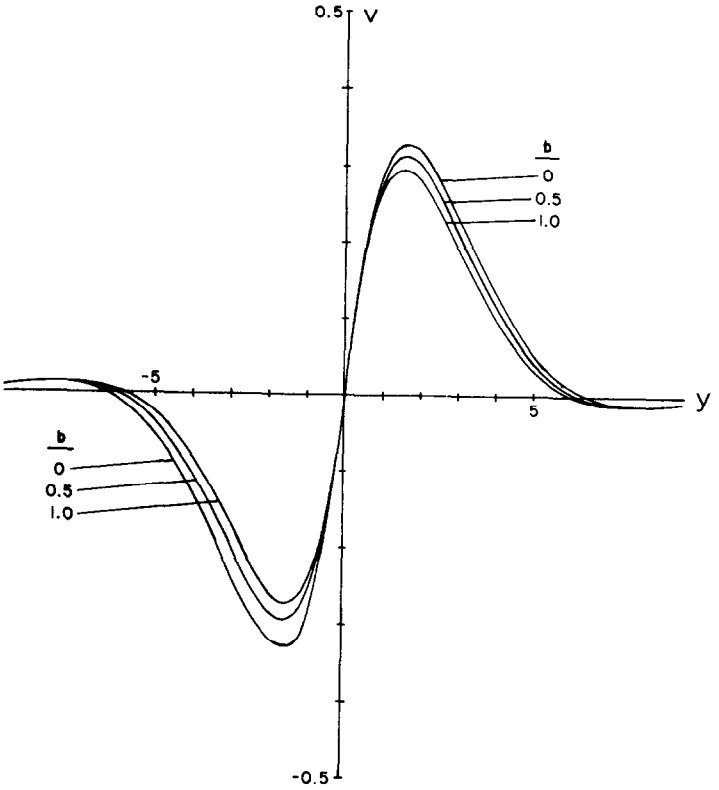

FIG. 3. Velocity profiles at mid-height as a function of cold reservoir stratification.

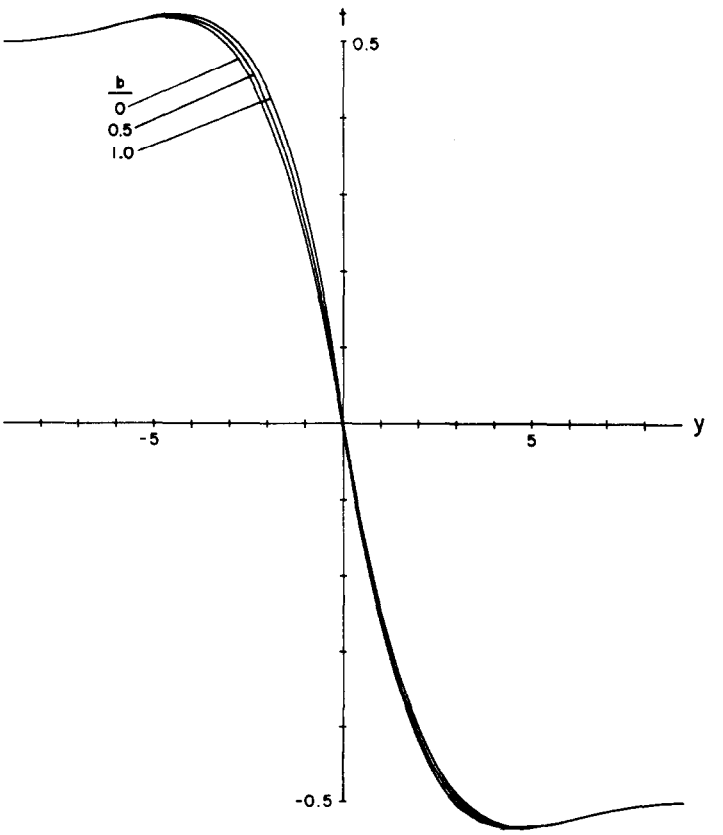

FIG. 4. Temperature profiles at mid-height as a function of cold reservoir stratification.

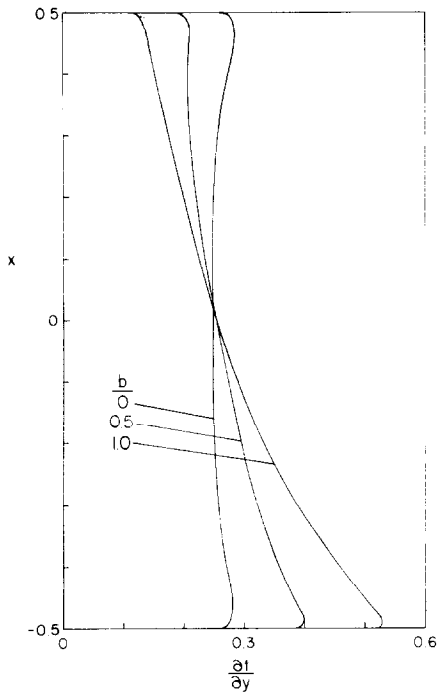

FIG. 5. Partition heat flux as a function of cold reservoir stratification.

creased stratification enhances the heat transfer between the fluid reservoirs. For stable boundary layers without secondary flows, the hottest fluid on the hot side at the temperature $\frac{1}{2}(a+1)$ must be as hot or hotter than the hottest fluid on the cold side at $t = \frac{1}{2}(b-1)$. The same must be true of the coldest fluid on each side. These two inequalities lead to the criterion for simple boundary layer flow that

$$|a-b| \leq 2. \tag{36}$$

In physical terms, a and b are the vertical temperature differences at each end, divided by the temperature difference between each end taken at mid-height. The magnitudes of a and b are related to the dimensions of the enclosure, to the extent that it requires a tall fluid reservoir to support a large vertical temperature difference. The stratification levels shown in Fig. 6 are typical of those found in systems subjected to natural heating and cooling.

3. EXPERIMENT

In parallel with the preceding theoretical study, we carried out an experiment in a water-filled enclosure heated at one end and cooled at the other. The overall temperature difference between the ends of the en-

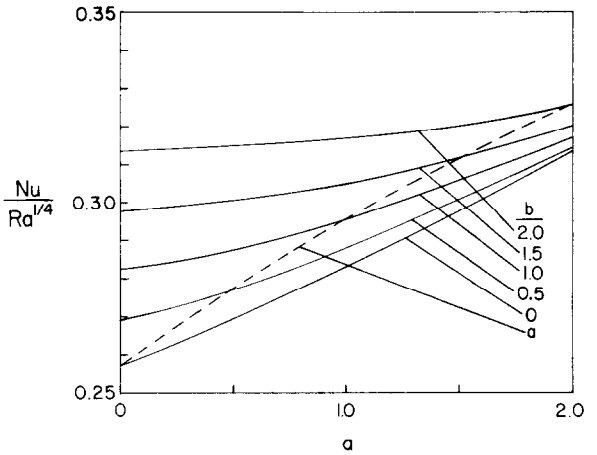

FIG. 6. Overall heat transfer as a function of thermal stratification in both reservoirs.

Table 1. $\hat{Nu}/\hat{Ra}^{1/4}$ as a function of reservoir stratification†

a \ b	0	0.5	1.0	1.5	2.0
0	0.2575	0.2690	0.2825	0.2975	0.3134
0.5	0.2690	0.2775	0.2879	0.3005	0.3143
1.0	0.2825	0.2879	0.2954	0.3048	0.3169
1.5	0.2975	0.3005	0.3048	0.3114	0.3204
2.0	0.3134	0.3143	0.3169	0.3204	0.3260

†These results are correlated within 0.5% by the formula

$$\hat{Nu}/\hat{Ra}^{1/4} = 0.257[1 + 0.02(a-b)^2][(1 + 0.505a)(1 + 0.505b)]^{0.17}.$$

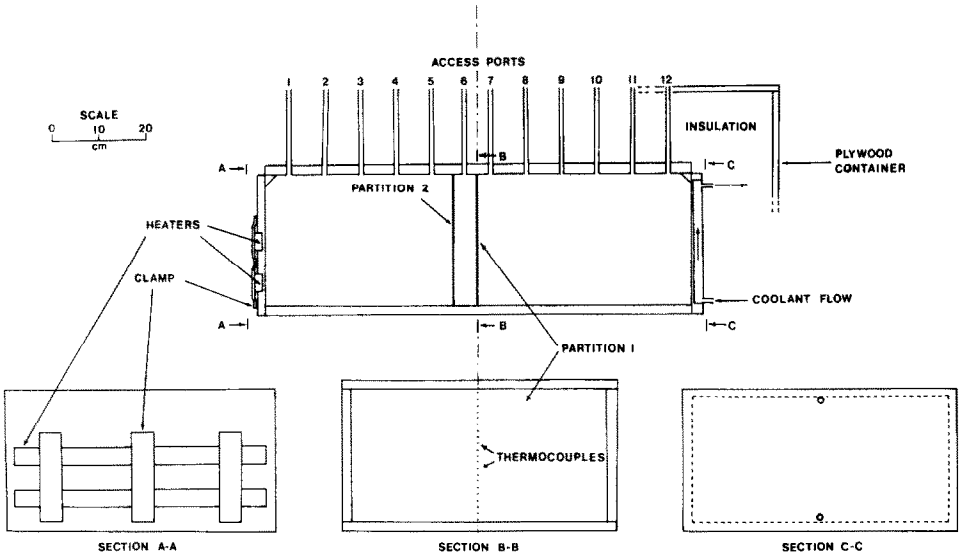

FIG. 7. Schematic scale-drawing of experimental apparatus.

closure varied in the range $6 - 35°C$, with the overall Ra varying in the range $10^9 - 10^{10}$. Measurements were made to determine the overall heat exchange, the temperature distribution in the fluid and along the partition(s), and the velocity profiles at the exit of the partition boundary layer. Water was chosen as the heat transfer medium because it allows one to use a scaled-down apparatus to produce the high Rayleigh numbers associated with typical building configurations. For example, $Ra = 1.6 \times 10^9$ corresponds to a building wall 2.4 m high, with a 1°C temperature difference across it.

3.1. *Apparatus*

Construction details of the experiment are shown in Fig. 7. The transverse cross-section of the box measured 27.9 × 54.6 cm, with a length of 91.4 cm. The box was constructed out of 1.9 cm-thick plexiglass sheet, insulated with 15 cm-thick fiberglass insulation, and then surrounded with an outer container of 1.3 cm-thick plywood. All joints were caulked or weatherstripped to minimize air-infiltration heat losses. The width of the inner enclosure was chosen to minimize three-dimensional effects, and the length to minimize any effects the end plates might have on the fluid behavior at the mid-line of the enclosure. The hot and cold ends were constructed of aluminum plates 1.9 cm-thick. The cold end was hollowed out to serve as a heat exchanger and connected to a refrigerator capable of controlling the coolant temperature to within $\pm 0.1°C$. Two 500 W strip heaters were connected in parallel and recessed into the hot end plate. All aluminum surfaces were sprayed with a thin layer of lacquer to inhibit oxidation. A constant-voltage transformer was used to limit the effects of diurnal swings in the building's electrical supply. Total power inputs varied from 50 to 600 W (328 – 3940 W/m^2).

Temperature measurements were made to within $\pm 0.5°C$, using 30 gauge type K (chromel – alumel) thermocouples. End plate temperatures and ambient temperatures were monitored throughout each data run. Partition and fluid temperature profiles were measured upon arrival at steady state. For the single partition measurements, 21 thermocouples were inserted in the aluminum partition on a vertical line midway between the lateral walls of the box. The thermocouple leads were fed through narrow horizontal slots in the partition which were later refilled with steel epoxy. The additional plate used in the double-partition experiments was equipped with six thermocouples arranged in a similar manner. Square apertures (28 × 28 cm) were built into the sides of the outer box (and insulated with removable blocks of rigid styrofoam) to allow visual observation of the boundary layers lining the vertical partition(s).

3.2. *Experimental procedure*

In general, the apparatus needed about 24 h to stabilize whenever the power setting was changed. Arrival at steady state was determined by monitoring the end plate temperatures. Within any given steady state, the maximum variations in temperature were $\pm \frac{1}{2}\%$ for the hot and cold ends and 4% for the air surrounding the apparatus. The power input was measured by monitoring heater voltage and current: this reading varied within 2%. The vertical temperature variation along the end plates was $\pm 3°C$ when the overall temperature difference was of the order of 25°C.

In order to minimize the thermal interaction of the apparatus with its surroundings, the coolant tempera-

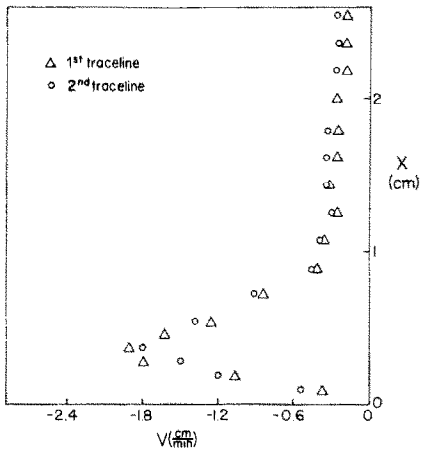

FIG. 8. Bottom boundary layer velocity measured inside the double partition.

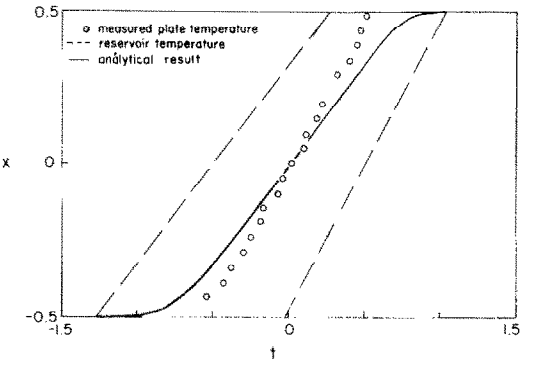

FIG. 9. Single partition temperature profile.

ture was set so that the mean operating temperature, $(T_H^* + T_C^*)/2$, was within $\pm 2°C$ of the ambient during the 'no partition' and 'single partition' measurements, and $\pm 5°C$ during the 'double partition' measurements. Multiple data runs were made at each power level to compensate for any variations due to the operating point of the apparatus. All physical properties of water were calculated at the mean operating temperature.

The overall heat-loss conductance of the fiberglass insulation was determined to be 1 W/°C, by running the experiment with a low power input until it reached steady state *without* any coolant flow. To estimate the effect that heat losses or gains would have upon calculation of the Nusselt number, the apparatus was modeled as having isothermal top, bottom, and side walls, the top and bottom temperatures being equal to the top and bottom fluid temperature inside the box and the sidewall temperature being taken equal to the fluid temperature at mid-height. Corrections due to heat loss were found to be necessary only in the case of the double partition measurements.

Temperature profiles in the water were measured by lowering a thermocouple probe through one of the access ports in the top of the box. The time constant of the probe was determined experimentally: it was found that 30 s were sufficient to allow the probe to stabilize before recording its output. Temperature profiles were measured near the ends of the box, halfway between the end and the partition, and on each side near the partition.

Velocities in the boundary layer on the bottom of the box were determined by analyzing streaklines produced by dropping potassium permanganate ($KMnO_4$) crystals through the top access ports. The movement of the streaklines was measured by taking pictures at measured time intervals. The velocity of the flow was then calculated by dividing the displacement of the streaklines by the elapsed time interval.

3.3. *Results*

Streakline measurements taken in the core region between the double partition are shown in Fig. 8. The plates were spaced 5.1 cm apart, which is ten times larger than the boundary layer thickness. As a result, distinct boundary layers were formed on each surface. The core showed no motion except for regions near the top and bottom walls. The velocity profile of the bottom boundary layer shown in Fig. 8 was determined by taking detailed pictures near the bottom of the box. The first set of points indicates velocities calculated after a 10 s interval, and the second set velocities calculated after a 20 s interval. The small nonzero velocity at larger values of X is a result of entrainment into the vertical boundary layer. The region between the double partition appears to behave

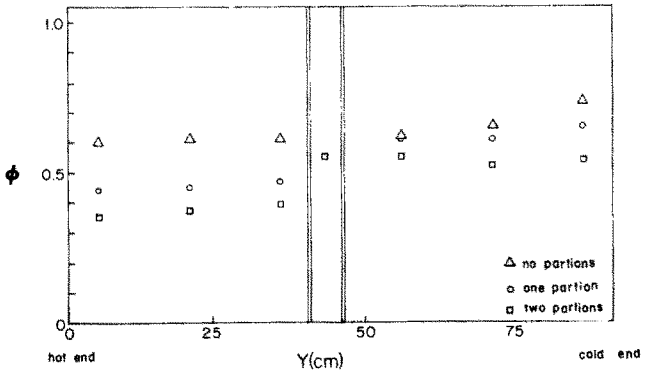

FIG. 10. Local temperature gradients.

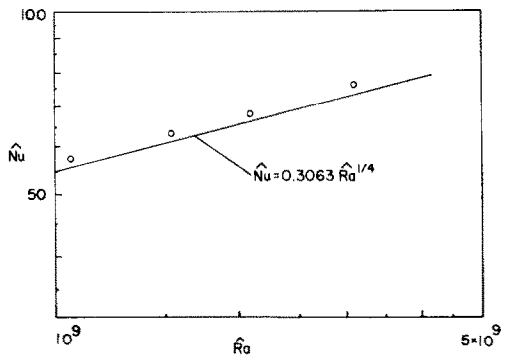

FIG. 11. Experimental measurements of overall heat transfer through a single partition.

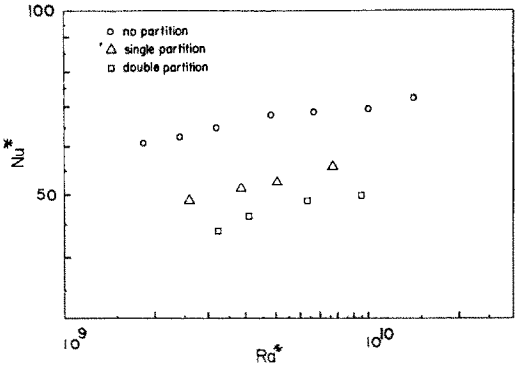

FIG. 12. Overall heat transfer as a function of the number of partitions.

much like a classical enclosure with isothermal walls. The bottom half of the cold boundary layer actively entrains fluid from the bottom half of the hot layer and the upper half of the hot boundary layer entrains fluid from the upper half of the cold boundary layer.

A comparison between measured temperature profiles on the single partition and the theoretical profile $t_0(x)$ derived in Section 2 is shown in Fig. 9. The discrepancy between the expected curve and the measured values is the result of heat conduction in the x-direction through the partition. This effect was assumed negligible in the derivation of the theoretical curve.

Figure 10 reports the vertical temperature variations recorded during the experiment. The quantity ϕ is the fluid temperature difference between the top and bottom of the box at a given location, divided by the maximum temperature difference in the box. The maximum temperature difference, ΔT_{max}, occurs between the top of the hot end and the bottom of the cold end. The gradients are larger on the cold side because the variation of fluid properties, particularly μ and β, makes it necessary to have a larger temperature difference to transfer the same amount of heat as is transferred by the hot end.

The vertical temperature gradients present in the fluid surrounding the partition were approximated by a linear least-squares-fit to the profiles observed on each end of the apparatus. The resulting gradients are represented in Fig. 9 by the dashed lines on either side of the experimental points and theoretical curve. In the case of the single partition, the gradients were found to be $a = 1.07 \pm 0.02$ on the hot side and $b = 1.53 \pm 0.08$ on the cold side. These experiment-based gradients were used to reconstruct the relationship between $\hat{Nu}$ and $\hat{Ra}$, shown as a solid line in Fig. 11. The agreement between the theoretical line and the experimental data is very good.

A compilation of the experimental Nusselt number measurements for zero, single and double partitions is shown in Fig. 12. Each of the points in the figure is an average of experimental values taken at constant power levels. The largest errors are associated with the double partition measurements with a Ra^* variation of 11% and a Nu^* variation of 9%. The remaining points have Ra^* variations of 9% and Nu^* variations of 5%. Figure 12 shows that the introduction of a second partition does not produce a proportional reduction in heat transfer. The first partition reduces heat transfer by a factor of 0.6 over having no partition, but the second partition only reduces the heat transfer by an additional factor of 0.8. The heat-transfer data of Fig. 12 are all correlated within 10% by the expression

$$Nu = 0.167(n+1)^{-0.61}\,Ra^{1/4} \tag{37}$$

where n is the number of vertical partitions. This correlation is consistent with the fact that $(1+n)$ represents the total number of boundary layer pairs (thermal resistances) encountered by the end-to-end heat flow.

4. CONCLUSIONS

In this paper we have reported a theoretical and experimental study of heat transfer through a single or a double partition which divides a fluid-filled enclosure into two differentially-heated chambers. By employing the Oseen linearization technique and assuming $Pr > 1$, we have showed analytically the effect of thermal stratification of the two chambers on the partition temperature and on the boundary layer counterflow which surrounds the partition. More importantly, however, we have determined the relationship between the overall heat transfer through the partition and the varying degrees of thermal stratification which may be present in the two adjacent chambers. This relationship is important in heat-transfer calculations for energy conservation in buildings and other insulation systems.

The experimental part of our study was designed to document the basic features of the natural circulation in the system and, at the same time, to verify the analytical conclusions of our theory. The experiment showed that the fluid is thermally stratified on both sides of the partition. It showed also that the temperature of the partition increases steadily with altitude. The net heat transfer between the two differentially-heated ends of the rectangular enclosure decreases as

more partitions are inserted. The net heat-transfer rate was shown to vary inversely with $(1 + n)$, where n is the number of vertical partitions. We showed also that our theoretical Nusselt number prediction (Fig. 6, Table 1) can be used with confidence as long as the thermal stratification degrees (a, b) are known.

Acknowledgements—This research was supported by the National Science Foundation, through grant ENG 79-20957. The authors thank Dean K. D. Timmerhaus for the early financial support of the construction phase, and Mr Karl Rupp and Mr Richard Cowgill for their part in constructing the apparatus and the instrumentation.

REFERENCES

1. S. Ostrach, *NACA Rep.* 1111 (1953).
2. E. M. Sparrow and J. L. Gregg, Laminar free convection from a vertical plate with uniform surface heat flux, *Trans ASME* **79**, 435 (1956).
3. B. Gebhart, *Heat Transfer*, Chap. 8, 2nd Edn. McGraw-Hill, New York (1971).
4. S. Ostrach, Natural convection in enclosures, pp. 161–227, in *Advances in Heat Transfer*, Vol. 8, Academic Press, New York (1972).
5. G. S. H. Lock and R. S. Ko, Coupling through a wall between two free convective systems, *Int. J. Heat Mass Transfer* **16**, 2087–2096 (1963).
6. R. Anderson and A. Bejan, Natural convection on both sides of a vertical wall separating fluids at different temperatures, *J. Heat Transfer* **102**, 630 (1980).
7. G. D. Raithby, K. G. T. Hollands and T. E. Unny, Analysis of heat transfer by natural convection across vertical fluid layers, *J. Heat Transfer* **99**, 287 (1977).
8. A. E. Gill, The boundary layer regime for convection in a rectangular cavity, *J. Fluid Mech.* **26**, 515 (1966).
9. A. Bejan, Note on Gill's solution for free convection in a vertical enclosure, *J. Fluid Mech.* **90**, 561 (1979).
10. R. Eichhorn, Natural convection in a thermally stratified fluid, *Progr. Heat Mass Transfer*, pp. 41–53 (1969).
11. Y. Jaluria and B. Gebhart, Stability and transition of buoyancy-induced flows in a stratified medium, *J. Fluid Mech.* **66**, 593–612 (1974).

TRANSFERT THERMIQUE DE CONVECTION NATURELLE SUR UNE OU DEUX PAROIS VERTICALES: THEORIE ET EXPERIENCE

Résumé—On étudie théoriquement et expérimentalement la convection thermique entre des parois verticales entourées par des fluides thermiquement stratifiés. La théorie est basée sur la méthode linéarisée d'Oseen. Les résultats analytiques montrent l'effet de la stratification thermique sur la température de partition, sur l'écoulement de fluide et sur le flux thermique. La relation entre le transfert thermique global (nombre de Nusselt) et les degrés de stratification sur les deux faces de la partition est déterminée. La partie expérimentale de l'étude confirme les configurations prévues analytiquement. En particulier, on montre que le calcul du nombre de Nusselt s'accorde très bien avec les mesures. On montre aussi que le transfert net entre les deux extrémités d'une enceinte rectangulaire est proportionnel à $(1 + n)^{-0.61}$ si n est le nombre de partitions verticales insérées au milieu de l'enceinte.

WÄRMEÜBERTRAGUNG DURCH EINZELNE UND DOPPELTE VERTIKALE WÄNDE BEI FREIER KONVEKTION: THEORIE UND EXPERIMENT

Zusammenfassung—Es wird theoretisch und experimentell die Wärmeübertragung durch vertikale Trennwände untersucht, die von thermisch geschichteten Fluiden umgeben sind. Die Theorie stützt sich auf die Oseen-Linearisierungsmethode. Die analytischen Ergebnisse zeigen den Einfluß der thermischen Schichtung auf die Temperatur der Trennwand, die Fluidströmung und den Wärmestrom. Es wird der Zusammenhang zwischen dem Gesamtwärmedurchgang (Nusselt-Zahl) und dem Grad der thermischen Schichtung auf beiden Seiten der Trennwand bestimmt. Der experimentelle Teil der Studie bestätigt die analytisch vorausbestimmten Merkmale der Wärmeübertragung. Insbesondere wird gezeigt, daß die theoretische Berechnung der Nusselt-Zahl sehr gut mit den experimentellen Messungen übereinstimmt. Weiterhin ergibt sich die Gesamtwärmeübertragung zwischen den beiden Enden eines rechteckigen Hohlraums proportional zu $(1+n)^{-0,61}$, wobei n die Zahl der in der Mitte des Hohlraums eingebauten vertikalen Trennwände ist.

ТЕПЛОПЕРЕНОС ЧЕРЕЗ ЕДИНИЧНУЮ И СДВОЕННУЮ ВЕРТИКАЛЬНЫЕ ПЕРЕГОРОДКИ ПРИ ЕСТЕСТВЕННОЙ КОНВЕКЦИИ. ТЕОРИЯ И ЭКСПЕРИМЕНТ

Аннотация — Теоретически и экспериментально исследуется теплоперенос через вертикальные перегородки, по обе стороны которых находятся термически стратифицированные объемы жидкости. В основу теоретического анализа положен метод линеаризации Озеена. Полученные результаты свидетельствуют о влиянии термической стратификации жидкости на температуру перегородки, динамику потока и величину теплового потока. Выведено соотношение между суммарным переносом тепла (число Нуссельта) и степенью термической стратификации по обе стороны перегородки. Полученные экспериментальные данные подтверждают результаты анализа. В частности показано, что расчетные значения числа Нуссельта хорошо согласуются с измеренными. Показано также, что величина результирующего переноса тепла между двумя стенками прямоугольной полости пропорциональна $(1 + n)^{-0.61}$, где n — число вертикальных перегородок, помещенных в центре полости.